analytical chemistry

Article

pubs.acs.org/ac

Microfluidic Device for Studying Controllable Hydrodynamic Flow Induced Cellular Responses

Chunhong Zheng, Xiannian Zhang, Chunmei Li, Yuhong Pang,* and Yanyi Huang*

Beijing Advanced Innovation Center for Genomics (ICG), Biodynamic Optical Imaging Center (BIOPIC), School of Life Sciences, College of Engineering, and Peking-Tsinghua Center for Life Sciences, Peking University, Beijing 100871, China

Supporting Information

ABSTRACT: Hydrodynamic flow is an essential stimulus in many cellular functions, regulating many mechanical sensitive pathways and closely associating with human health status and diseases. The flow pattern of blood in vessels is the key factor in causing atherosclerosis. Hemodynamics has great effect on endothelial cells' gene expression and biological functions. There are various tools that can be used for studying flow-induced cellular responses but most of them are either bulky or lack precise controllability. We develop an integrated microfluidic device that can precisely generate different flow patterns to human endothelial cells cultured on-chip. We monitored cell morphology and used small-input RNA-seq technology to depict the transcriptome profiles of human umbilical vein endothelial cells under uni- or bidirectional flow. Such integrated and miniatured device has greatly facilitated our understanding of endothelial functions with shear stimulus, not only providing new data on the transcriptomic scale but also building the connection between cell phenotypic changes and expression alternations.

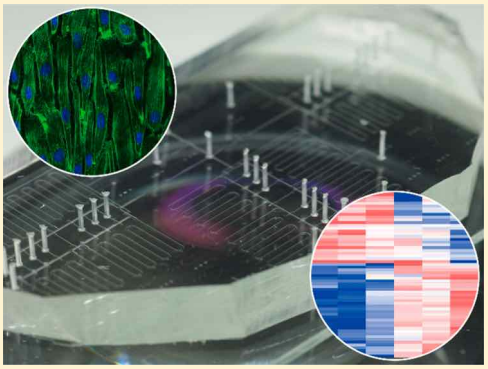

Shear stress, especially the flow of body fluids, is one of the key factors that physically stimulates cells in a living organism. Such stimulus has been known to regulate many essential genes highly associated with necessary cell functions as well as with diseases. For example, atherosclerosis preferentially occurs in the arterial regions exposed to the stimulations from low and oscillatory shear stress.[1] Hemodynamics has been found crucial to cardiovascular health. Unidirectional flow (UF) is the dominant flow pattern in healthy arteries, while bidirectional flow (BF), a simplified pattern of chaotic flow, will cause endothelial dysfunction, such as inflammatory responses, higher migration rate, apoptosis, and angiogenesis.[2] These pathological responses, along with the immune cells attached to the endothelium, begin the cascade of intimal hyperplasia and gradually develop into atherosclerotic plaque.[3]

To study the function of shear-stress, or flow patterns, on the genetic and biochemical alternations of endothelial cells, many in vitro methods have been developed to mimic the flow conditions in vivo. For example, cone-and-plate model utilizes a small-angled cone soaking in culturing medium and spinning above a Petri-dish with confluent endothelial cells.[4] Parallel plate model consists of a flow chamber with inner surface covered by endothelial cells while culturing medium was circulated through the flow chamber by an external pump.[5] These flow models have been adapted by many researchers to provide important insights regarding shear-sensitive cellular processes. However, some disadvantages, including high consumption of precious reagents, nonuniformity of the flow profile, and limited reproducibility, seriously reduce the applicability and robustness of these methods. Recently, various microfluidic or lab-on-a-chip applications have been presented to investigate the mechanical and biochemical response of endothelial cells to shear stress, majorly focusing on morphology and chemotaxis.[6−10] The microfluidic stretch chip is also developed to deliver stress to vascular cells to mimic the hemodynamic microenvironment of blood vessels in vivo, but with totally different mechanism from flow-induced shear stress.[11]

In this paper, we present a microfluidic approach that uses an integrated device to apply UF and BF to human umbilical endothelial cells (HUVECs) with high precision and accuracy. With this device, we focus on shear-sensitive morphological and whole transcriptome responses. Besides profiling the gene expression landscapes of HUVEC under UF and BF and identifying differentially expressed genes that are sensitive to flow patterns, we also utilize this platform to explore the alternative splicing preference under UF and BF. By characterizing flow-sensitive genes and investigating flow-dependent alternative splicing patterns, we provide new insight of the mechanical sensitive genome-wide regulatory networks. This microfluidic chip can be further scaled up to a higher throughput fashion and be integrated into other devices to provide a promising platform for screening drugs to effectively treat cardiovascular diseases.

Received: January 2, 2017
Accepted: February 22, 2017
Published: February 22, 2017

DOI: 10.1021/acs.analchem.7b00013
Anal. Chem. 2017, 89, 3710−3715

EXPERIMENTAL SECTION

Flow Chip Fabrication. We fabricated the microfluidic flow chip by multilayer soft lithography.[12] Briefly, the control layer master mold was made from a 25 μm-thick layer of SU8-2025 photoresist (MicroChem, MA). The photoresist was spin-coated, preheated at 65 °C for 3 min and 95 °C for 5 min on silicon wafer, and UV-exposed under a printed high-resolution mask. After the pattern was developed, the mold was postbaked at 65 °C for 5 min and 95 °C for 10 min for hardening. The fabrication process of the master mold of fluid layer had two major steps: First, a 50 μm-thick layer of P4620 photoresist (AZ Electronic Materials, NJ) was made by four times spin-coating on top of the wafer, preheated at 65 °C for 1 min, 95 °C for 7 min, 115 °C for 15 min, and then UV-exposed. The wafer was developed and postbaked from 40 to 220 °C at the ramp 20 °C/h to facilitate sealing of the valves by rounding the channel. Then, a 25 μm-thick fluid layer of channels was made from the SU8-2025 photoresist by a similar method with the control layer and aligned with another mask that has only a part of the channels printed and UV-exposed. Both master molds were fumigated with chlorotrimethylsilane for 10 min for easier peeling off the PDMS slab. After the fumigation, 5:1 ratio mixed PDMS (Sylgard 184, Dow Corning, Michigan) was poured into a Petri-dish with control channel master mold in the bottom to the thickness of about 3 mm. The 23:1 ratio mixed PDMS was mixed and spin-coated on the fluid channel mold at 1000 rpm for 60 s. Both PDMS-coated molds were baked at 80 °C for 30 min. Then the control channel slab was peeled off from the mold, carefully aligned to the fluid channel mold after puncturing holes for connecting hoses to the chip, and baked at 80 °C for 60 min. The two assembled layers were peeled off from the fluidic channel mold, and the rest of the holes were punched for the access to the fluidic channel. Finally, the PDMS slab was placed on a glass slide that was spin-coated with PDMS (ratio 20:1) at 1300 rpm for 60 s and baked at 80 °C overnight for complete sealing (Figure S1).

Cell Handling and Chip Preparation. The primary human umbilical vein endothelial cells (HUVECs) were kindly provided as a gift from Xingyu Jiang lab (National Nanoscience and Technology Center, China). Cells were cultured with Medium 199 (Invitrogen) supplemented with 5% FBS (Sciencell), 1% Pen-Strep solution (Invitrogen), and 1% endothelial cell growth supplement (Sciencell). Cells between passage 2 and 7 were used for all the experiments. Before transferring the HUVECs to the flow chip, the entire fluidic channels were incubated with 200 μg/mL fibronectin (Invitrogen) for 2 h at room temperature. HUVECs were detached from T25 flasks with 0.25% trypsin−0.1% EDTA solution and suspended in 20 μL of M199 medium. Then the cell suspension was introduced to fill the fluid channels when the "pump valves" were closed. The cells were incubated at 37 °C for 2 h for the HUVECs attaching to the bottom of the channels. The unattached HUVECs were washed away by M199 medium, and the adherent cells were cultured for another 4 h before applying flow.

***KLF2* siRNA Knock-down.** siRNA targeting *KLF2* (Sense, 5′-GUG ACU GAC AAA UAU UGU ATT-3′; Anti-Sense, 5′-UAC AAU AUU UGU CAG UCA CTT-3′) and nontargeting control siRNA (Sense, 5′-UUC UCC GAA CGU GUC ACG UTT-3′; Anti-Sense, 5′-ACG UGA CAC GUU CGG AGA ATT-3′) were synthesized and transfected with Lipofectamine 2000 (Invitrogen) to HUVECs at a final concentration of 200 nM. At a time 24 h after the transfection, HUVECs were transferred to the flow chip for flow stimulation.

Cell Fluorescence Staining and Confocal Imaging. After 24 h flow treatments, the microfluidic channels were rinsed with PBS and then the HUVECs were fixed in 4% paraformaldehyde for 15 min at room temperature. The fixed cells were washed with PBS buffer for 5 min, and 1 μg/mL Alexa Fluor 555 conjugated phalloidin (invitrogen) with 0.1% Triton X-100 and 1 mg/mL BSA were filled into the fluid channels and incubated for 30 min at 37 °C. Then the cells were washed with PBS for 5 min and incubated with 3 μM DAPI solution for 10 min at room temperature. After 5 min of PBS wash, cell images were taken with TCS-SP5II confocal microscope (Leica) with a 63× NA 1.20 water-immersion objective (Leica).

RNA Extraction and RT-qPCR. After flow treatment for 24 h, HUVECs were incubated with 0.25% trypsin−0.1% EDTA solution at 37 °C for 3 min to detach from the surface of fluid channels. Then the cells were centrifuged and washed for three times with PBS. A volume of 700 μL of Qiazol (Qiagen) was added to lyse the cells, and miRNeasy kit (Qiagen) was used with the manufacturer's protocol to extract the total RNA from these flow-treated HUVECs. RNA was eluted with 25 μL of RNase-free water. Typically, 100 ng of total RNA could be harvest from each single flow channel, which contains about 10 000 cells. We used SuperScriptIII First-Strand Synthesis SuperMix (Invitrogen) and random hexamer to convert RNA to cDNA with the manufacturer's protocol. Brilliant II SYBR Green qPCR Mastermix (Agilent) was used in 25 μL of qPCR reactions in 96-well plate with ABI 7500 real-time PCR machine (Life Technologies). The expression level of each gene was normalized with 18S rRNA and calculated by the ΔΔCt method. Primer sequences can be found in Table S1.

Transcriptome Sequencing and Alternative Splicing Analysis. An amount of 10 ng of total RNA samples was reverse-transcripted and preamplified with the Ovation RNA-Seq system (NuGEN) to generate microgram quantities of cDNA prior to the next generation of sequencing of the transcriptome. In total, 3 μg of preamplified cDNA samples was sheared using Covaris sonication and the majority of fragments between 150 and 200 bp were selected. Multiplex libraries were prepared according to standard procedure of NEBNext kit, including end repair, dA-tailing, adaptor ligation, and PCR enrichment, and then constructed libraries were run on the illumina HiSeq 2000 instrument. Sequence data were subjected to the whole transcriptome analysis. The raw reads were mapped to the human reference genome (version hg19) with TopHat (version v2.0.14).[13] The gene expression level is normalized as FPKM (fragments per kilobase of exon per million fragments mapped), which was estimated using cufflinks (version v2.2.1).[13] Significantly differentially expressed genes were detected using edgeR,[14] which received the raw read counts, and then estimated the dispersion and fit negative binomial models. The generalized linear model (GLM) quasi-likelihood (QL) F-test was done, and the genes with fold change >2, p-value <0.05, and FDR < 0.05 were considered to be significantly expressed differentially. For alternative splicing analysis, the junction read counts between exons in each isoform were exported in default TopHat pipeline.[15] The junction reads were grouped by their donor site for each treatment. The candidate AS events required at least two acceptors for the same donor with at least in total 30 junction reads covered, respectively. The significant AS events were

DOI: 10.1021/acs.analchem.7b00013
Anal. Chem. 2017, 89, 3710−3715

determined using Bonferroni-corrected Fisher's exact test (corrected $p < 0.05$) on the total read counts between donor and its corresponding two acceptors.

RESULTS AND DISCUSSION

Functions of the Microfluidic Chip. This PDMS-based microfluidic flow device (Figure 1a), fabricated with two layers

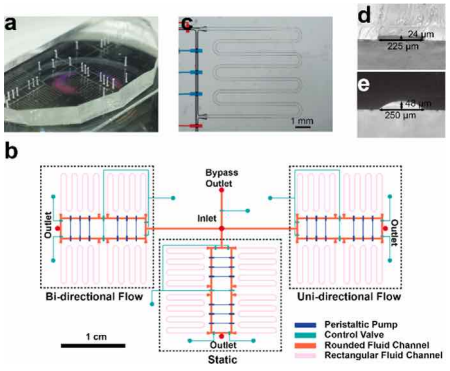

Figure 1. Microfluidic flow-chip design. (a) The photograph of microfluidic device. (b) Schematic diagram of the full microfluidic flow chip. The chip size is about 6.5 cm × 3.5 cm. Three different flow profiles, including bidirectional flow, static, and unidirectional flow, are designed in parallel regions on one chip with four replicated flow units in each region. Channels shown in red and pink are fluid channels for cell culture and applying flow, while channels shown in dark-green and blue are control channels. (c) The photograph of one flow unit on-chip. (d) The rectangular fluid channel part fabricated with SU8 is 24 μm in height and 225 μm in width. (e) The rounded fluid channel part fabricated with AZP4620 photoresist and hard-baked to form a rounded cross-section is about 48 μm in height and about 250 μm in width.

of microchannels using multilayer soft lithography method,[12] contains three identical regions to treat the cells with BF, UF, or static (ST) conditions in parallel (Figure 1b). The flow channels, on the bottom of the chip, are composed of two channel types (Figure 1c); the rectangular fluid channels are used for culturing HUVECs with lower height (about 24 μm) (Figure 1d) and the rounded fluid channels are used for applying different flow patterns with higher height (about 48 μm) (Figure 1e). In each single flow unit, the control layer consists of five monolithically integrated pneumatic valves[16] that can open or shut the overlying flow channel by applying a pressure to deform the thin membrane between two layers of channels (Figure 2a). While valves 1 and 2 are shut, a closed loop is formed. Valves 3, 4, and 5 can be sequentially actuated to act as a peristaltic pump[12] that controls the direction and velocity of medium flow. Both UF and BF can be simply achieved by programming the actuation sequences of these three valves. All processes were carried out on chip, including culturing cells and applying flow (Figure 2b). Cell suspension was introduced to the fluid channels and after they were confluent, we shut valves 1 and 2 to form the closed loop for circulation of culture medium. The states of the "pump valves" 3, 4, and 5 are cycled in the following "open (1)−close (0)" order: 110, 010, 011, 001, 101, 100, aiming to drive the flow in one direction. To perform BF, we switch the open to 0 and close to 1, thus the flow direction can be reversed. In each unit, we cultured about 10 000 HUVECs with 1 μL of medium, which was replaced every 2 h by fresh medium to keep the cells healthy. After 24 h of specific flow treatment, cells were

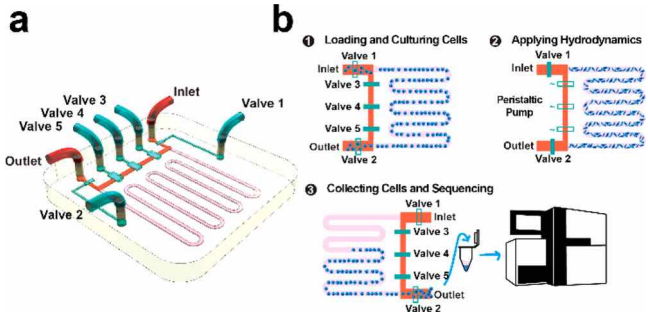

Figure 2. Microfluidic flow-chip can apply unidirectional flow (UF) and bidirectional flow (BF) to cultured HUVECs. (a) Schematic diagram of one flow unit on-chip. (b) Operational steps of microfluidic chip. Step 1: load HUVECs into fluid channels and culture cells for attachment. Step 2: Apply different flow profiles to HUVECs in a closed loop with peristaltic pump. Step 3: Collect cells for future biological procedure.

collected from the chip and total RNA was extracted for further processes and analyses.

Shear Stress Calculation. We applied different shear stress to endothelial cell monolayer in an attempt to approximate physiological conditions. For the laminar shear situation, we applied unidirectional flow. Given the preferential occurrence of oscillatory shear condition at the branched, bifurcated, and curved arteries, which is defined as both low shear stress and forward−reverse flow cycle pattern,[17] we applied the bidirection flow with a lower shear stress for the oscillatory shear condition (half the value of the unidirectional flow). As the cell culturing microchannel was fabricated into the rectangular shape, the shear stress in the microchannel was determined as

$$\tau = 12\frac{Q\mu}{h^2 w}$$

where Q is the volume flow rate, μ is the liquid's viscosity, h and w are the height and width of the microchannel, respectively. In the flow chip, for UF treatment, we used 20 ms intervals between each of the "pump valves" states so that the mean velocity was about 2 mm/s. For BF treatment, we used 50 ms intervals to achieve a mean velocity of about 1 mm/s and switched the directions every 2 s based on previous work[18] (i.e., the oscillatory flow frequency is 0.5 Hz). Since the height of microchannel was 24 μm, the width was 225 μm, and μ equaled to 1.2 mPa, the shear stress was calculated to 4 dyn/cm^2 for UF and 2 dyn/cm^2 for BF. Although the shear stress for UF in microfluidic channel was much lower than that in the cone-and-plate system (15 dyn/cm^2), endothelial cells under this stimulation had shown distinct phenotype, both on morphology and physiology.

Morphological Profile of HUVECs under Different Flow Patterns. It has been well-known that endothelial cells are mechanically sensitive and could be regulated by blood flow pattern.[4] To investigate the hydrodynamic effects on morphology of endothelial cells, we applied different flow patterns to confluent HUVECs on our microfluidic device and recorded their appearance at different time points. We observed time-dependent cell shape changes both in straight and bent microchannels after UF treatment compared to BF or ST conditions (Figure 3a and Figure S2). At the 12 h time point, endothelial cells show the tendency of elongation, and at the end time point (24 h), the tendency became more obvious. The

DOI: 10.1021/acs.analchem.7b00013
Anal. Chem. 2017, 89, 3710−3715

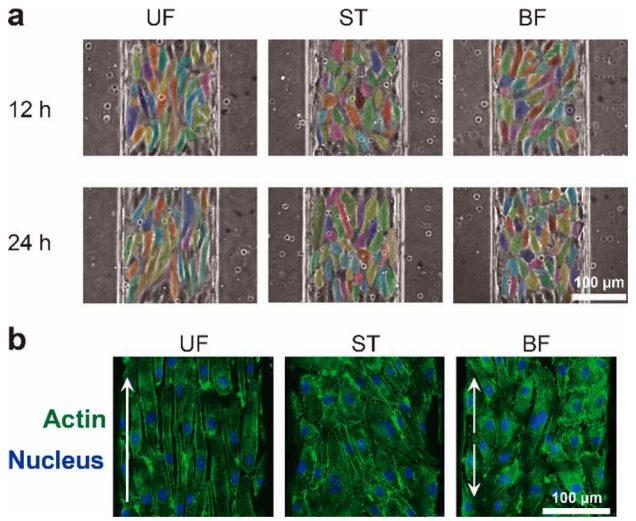

Figure 3. Morphology profile under different flow patterns. (a) Phase contrast images show the shape of HUVECs cultured in straight channel under different flow conditions for 12 or 24 h. The cell bodies were labeled with different colors. (b) After 24 h flow treatment, confocal fluorescent images of actin (green) and nucleus (blue) are taken. Cells are applied to UF treatment, static culture condition (ST), or BF treatment. Arrows indicate the flow directions. Scale bar, 100 μm.

most obvious changes in cell shape were also observed by confocal fluorescent images of actin filaments after 24 h flow treatment (Figure 3b and Figure S3). We further calculated the parameter of shape index (a measurement of how circular an object is, with a value between 0 and 1, and 1 indicates a circular shape) of HUVECs under different flow patterns and found that UF-treated HUVECs showed a much smaller shape index, indicating these cells with a more elongated shape. The fact that no significant difference of shape index between ST and BF was observed suggested that BF flow had no direct effects on shape adjustment of cells (Figure 4a). Next we examined the orientation of HUVECs with the angles between

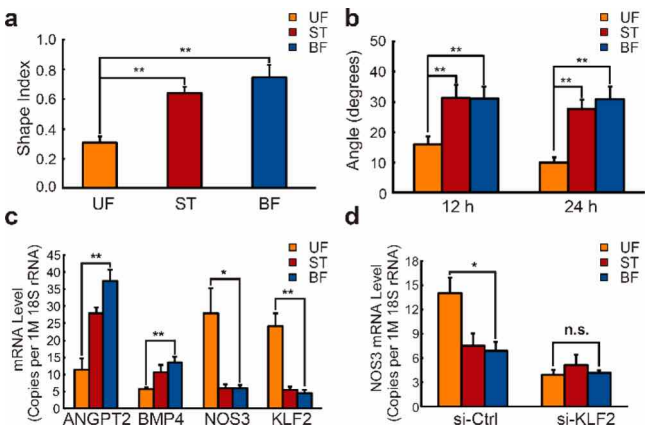

Figure 4. Shape index and gene expression profile under different flow pattern. (a) Shape index of HUVECs are analyzed after 24 h of different flows. (b) Angle between the long axis of HUVECs and the flow direction are analyzed after 12 and 24 h of different flows. (c) Expression level of several well-known flow-sensitive genes verified by qPCR after 24 h of different flow conditions. (d) Increase of UF-induced *NOS3* level is inhibited by *KLF2*-targeting siRNA. *, $p < 0.05$; **, $p < 0.01$; n.s., not significant.

the long axis of cells and the flow direction as well as the fluorescent images, which exhibited the orientation of cells' actin filaments. Cells with a significantly smaller angle and much more obvious actin alignment under UF condition than under other two conditions indicated that HUVECs had been promptly orientated in parallel to the flow direction under UF pattern (Figure 4b). These results suggest that flow pattern generated by microfluidic device sufficiently affect the HUVECs' morphology profile, consistent with previous reports that laminar flow would lead to the endothelial cells' morphological adaptation and actin reorganization,[19] and all the cell responses take only a few hours. In addition, the viability of the cells in unidirectional flow condition is much better than that in BF and ST, just as previous work that exposure to oscillatory would induce the apoptosis of endothelial cells.[20]

Gene Expression Profile of HUVECs under Different Flow Patterns. Clearly, such dramatic flow-dependent morphological changes should have been driven by active responses of certain mechanosensitive pathways and the interplay between them. To further investigate the flow effects on gene regulation, we harvested the chip-cultured HUVECs after 24 h of exposure to specific flow patterns, extracted total RNA, and performed RT-qPCR of known flow-sensitive genes. We confirmed that the expression level of pro-inflammatory genes bone morphogenetic protein 4 (*BMP4*, a mechanosensitive and pro-inflammatory protein)[18] and angiopoietin-2 (*ANGPT2*, regulating the vessel stabilization)[21] decreased while that of antiatherogenic genes endothelial nitric oxide synthase (*NOS3*, the endothelial cell specific gene)[22] and krüppel-like factor 2 (*KLF2*, regulating key genes involved in the endothelial response to inflammation)[23] increased under UF, compared to BF-treated HUVECs (Figure 4c). We further performed RNA interference to reveal the relationship between *KLF2* and *NOS3* with the microfluidic chip as well. When the *KLF2* was knocked down, both the flow-induced gene expression changes of *KLF2* and *NOS3* were blocked, confirming the effect of *KLF2* on regulation of *NOS3* expression as previous reported[24] (Figure 4d and Figure S4).

We then carried out RNA-seq to study the whole transcriptome changes of HUVECs after 24 h of UF-, BF-, and ST-treatments. Biological triplicates, with each of 10 ng of total RNA, were used to generate at least 25 million paired-end reads using an Illumina Hiseq sequencer. By comparing the UF- with BF-treated mRNA expression profiles, we identified 103 genes that were differentially expressed with high significance under different flow conditions, including those four previously confirmed flow-sensitive genes *ANGPT2*, *BMP4*, *KLF2*, and *NOS3* (Figure 5a and Table S2). Among these genes, 68 were significantly upregulated and 35 were downregulated when exposed to UF (Figure S5). We also performed RT-qPCR for 12 genes from another set of samples and validated the RNA-Seq results (Figure 5b). It is noticed that both morphology and gene expression are similar between BF and ST conditions, suggesting endothelial cells under ST are also deviated from normal status and the presence of laminar shear stress is very vital for endothelial cells function.[25]

Flow-Dependent Biological Functions. We further analyzed the interaction between these differentially expressed genes and their possible biological functions related to the flow sensitivity. Gene ontology (GO) analysis showed strong enrichment on two groups (Figure 5c). One group is highly related to cardiovascular system development, blood vessel

DOI: 10.1021/acs.analchem.7b00013
Anal. Chem. 2017, 89, 3710−3715

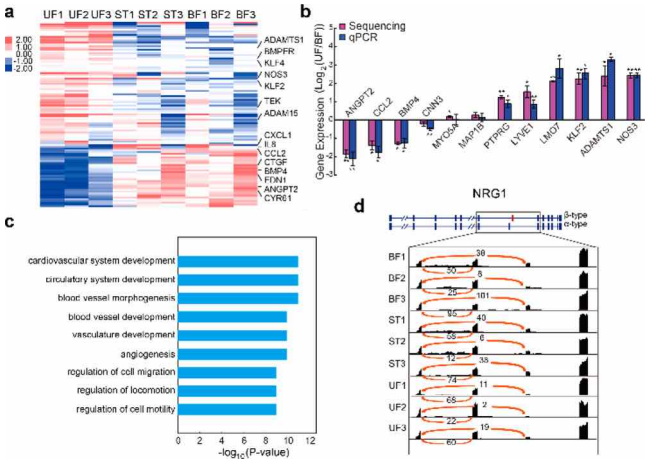

Figure 5. Flow-sensitive gene expression change and alternative splicing events revealed by RNA-seq after 24 h of UF-, ST-, or BF-treated HUVECs. (a) Heatmap showing differentially expressed mRNAs between UF and BF-treated HUVECs. (b) Validation of RNA-seq results by qPCR. *, $p < 0.05$; **, $p < 0.01$; $n = 3$. (c) Gene Ontology (GO) analysis of differentially expressed genes under different flow patterns. (d) Flow-sensitive alternative splicing events in NRG1.

morphogenesis, and angiogenesis. There are 14 common genes that engaged in all those processes, including shear sensitive genes *BMP4*, *ANGPT2*, and *NOS3*. In addition, chemokine *CCL2*, which can attract monocytes and is involved in the inflammatory cell recruitment,[26] was found with higher level of gene expression under BF stimulation compared to UF. The genes *CTGF* and *CYR61*, which can promote the growth and migration of endothelial cells and regulate angiogenesis, also showed flow-pattern-dependent expression. The fact that the expression of gene *CTGF* is a little higher under the BF stimulation agrees well with previously reported work[27] (Figure S6). The other group, containing 18 differentially expressed genes, is enriched in the cell motility related pathways, including regulation of cell migration, locomotion, and cell motility. Among these genes, *KLF4*, similar to *KLF2*, conferring athero-protective properties to the endothelial cell,[28] expressed higher under UF. Moreover, chemokine *CXCL1*,[26] which has great chemotactic activity for neutrophils and plays an important role in inflammation, displayed a 2-fold higher expression level under the BF stimulation (Figure S7).

To analyze the closeness of relationship among all differentially expressed genes, we plotted a functional clustering diagram with STRING10 method[29] (Figure S8). In this network map, angiogenesis and motility processes also appeared to be the main functional modules and formed tightly connected clusters. The eight-shared genes, including *BMP4*, *BMPER*, *TEK*, *ADAM15*, *IL8*, *EDN1*, *ANGPT2*, and *CYR61*, are major hubs in the network and play important roles in hydrodynamic responses (Figure S9). These results indicate the capability of microfluidic hydrodynamic control to allow for precise profiling of flow-sensitive transcriptome.

Flow-Dependent Alternative Splicing. Besides the difference of expression level, high-depth RNA-seq provides sufficient data sets for systematically analyzing flow-dependent alternative splicing (AS), which often plays an important role in gene regulation.[30] We detected AS events with RNA-seq data and quantified the various isoforms through identification and counting of specific junction reads between exons. We screened out two genes NRG1 and IFI44 with distinct isoform ingredients between UF and BF treatments, and the paired *t* test *p*-value is 0.025 and 0.026, respectively. The most evident AS events is in *NRG1*.[31] *NRG1* contains several domains, among which the EGF-like domain is known to be critical for its function. AS produces two types of EGF-like domains, α- and β-type, and determines receptor affinity. Typically, *NRG1* with a β-type EGF-like domain is 10−100 times more potent than α-type one. In our assay, ST and BF-treated HUVECs contain ∼40% of β-type while with UF treatment this ratio is 15% (Figure 5d). We verified the existence of AS in NRG1 and quantified NRG1 α- and β-type EGF-like domains using one set of samples (Figure S10a,b), confirming that different flow pattern indeed affects the activity of *NRG1* by isoform structure regulation under the similar expression level. Another notable AS event is in *IFI44*,[32] a less examined gene also known as *MTAP44*. This gene may play a role in regulating microtubule aggregation. Three isoforms have been detected. Iso1 contains full exons set, while Iso2 skips exon1 and Iso3 skips exon2. The Iso2 and Iso3 events significantly increased under UF stimulation compared to BF and ST (Figure S10c). However, unlike the substantial variance of expression level, the flow-induced AS is very subtle and may only be unveiled by highly precise flow stimulation through our microfluidic approach.

CONCLUSIONS

In this study we demonstrated an integrated microfluidic approach to investigate the mechanical response of endothelial cells from physical and biomedical perspective. Microfluidic flow chip could provide an ideal microenvironment to mimic both physical confinement and flow pattern of physiological condition for HUVECs, based on its most important advantage of the small volume-to-cell ratio of the culture-and-flow-loop chamber, enabling the concentration of cell secreted cytokines being maintained at a level close to the mimic of physiological conditions. In the microculturing environment, HUVECs show the same characteristics of different responses to hydrodynamics as in vivo, specifically displaying alignment along the flowing direction and elongated shapes under the UF pattern stimuli. A total of 103 differentially expressed genes between UF and BF are supposed to be candidate targets for understating the underlying mechanisms of atherosclerosis. The core Gene Ontology terms are related to angiogenesis and motility process, indicating the key biological process that endothelial cells are engaged in when responding to mechanical stimuli. Notably alternative splicing preferences are found under different flow stimulation, suggesting flow patterns' effects on isoform structure regulation.

This integrated microfluidic device has enabled the linkage study between the morphology and transcriptome changes of endothelial cells upon the hydrodynamic stimulation with precisely controlled flow patterns. With this linkage we are able to supply the mechanical sensitive genome-wide regulatory networks, with high accuracy and sensitivity, for future exploration on the mechanisms of atherosclerosis. Such device may also provide an important platform for further screening of drugs to treat cardiovascular diseases.

ASSOCIATED CONTENT

Supporting Information

The Supporting Information is available free of charge on the ACS Publications website at DOI: 10.1021/acs.analchem.7b00013.

DOI: 10.1021/acs.analchem.7b00013
Anal. Chem. 2017, 89, 3710−3715

Schematic of chip-making procedure; morphology profile under different flow pattern; confocal images of HUVECs under 24 h exposure to hydrodynamics stimulations with different flow-patterns; expression of *KLF2*; heatmap showing differentially expressed mRNAs between UF- and BF-treated HUVECs; overlapped genes related to blood vessel function and morphogenesis process; overlapped genes related to cell motility; closeness of relationship of 103 differentially expressed genes based on the functional roles in biological pathways, analyzed with STRING10 network diagram; Venn diagram showing the sharing genes and specific genes between motility related biology process and angiogenesis related biology process; flow-sensitive alternative splicing event of NRG1 and IFI44; primer sequences for RT-qPCR; and mRNA expression (FPKM) under different flow patterns (PDF)

AUTHOR INFORMATION

Corresponding Authors

*E-mail: pangyuhong@pku.edu.cn.

*E-mail: yanyi@pku.edu.cn.

ORCID

Yanyi Huang: 0000-0002-7297-1266

Author Contributions

C.Z. and X.Z. contributed equally. C.Z, Y.P., and Y.H conceived the project. C.Z, C.L., and Y.H conducted the experiment. C.Z and X.Z performed the data analysis. C.Z, X.Z., Y.P., and Y.H wrote the manuscript.

Notes

The authors declare no competing financial interest.

ACKNOWLEDGMENTS

The authors thank Dr. Fuchou Tang, Dr. Wensheng Wei, Dr. Hanjoong Jo, and Dr. Jianzhong Xi for fruitful discussions, Bingxiao Feng, Haiwei Qiu, Zhilong Yu, and Mingyu Yang for their help on experiments and data analysis, and Dr. Yun Zhang and the High-Throughput Sequencing Center of Peking University at BIOPIC for assistance with Illumina sequencing. This work was supported by Beijing Advanced Innovation Center for Genomics, Ministry of Science and Technology of China (Grants 2015AA0200601 and 2016YFC0900100) and National Natural Science Foundation of China (Grants 21327808 and 21525521). Dr. Chunhong Zheng is supported by Postdoctoral Scholarship of Peking-Tsinghua Center for Life Sciences.

REFERENCES

(1) Heo, K.-S.; Fujiwara, K.; Abe, J. *Mol. Cells* **2014**, *37*, 435−440.

(2) Chiu, J.-J.; Chien, S. *Physiol. Rev.* **2011**, *91*, 327−387.

(3) Ross, R. *N. Engl. J. Med.* **1999**, *340*, 115−126.

(4) Dewey, C. F., Jr.; Bussolari, S. R.; Gimbrone, M. A., Jr.; Davies, P. F. *J. Biomech. Eng.* **1981**, *103*, 177−185.

(5) Frangos, J. A.; Eskin, S. G.; McIntire, L. V.; Ives, C. L. *Science* **1985**, *227*, 1477−1479.

(6) Rossi, M.; Lindken, R.; Hierck, B. P.; Westerweel, J. *Lab Chip* **2009**, *9*, 1403−1411.

(7) Chin, L. K.; Yu, J. Q.; Fu, Y.; Yu, T.; Liu, A. Q.; Luo, K. Q. *Lab Chip* **2011**, *11*, 1856−1863.

(8) Shamloo, A.; Ma, N.; Poo, M.; Sohn, L. L.; Heilshorn, S. C. *Lab Chip* **2008**, *8*, 1292−1299.

(9) Shao, J.; Wu, L.; Wu, J.; Zheng, Y.; Zhao, H.; Jin, Q.; Zhao, J. *Lab Chip* **2009**, *9*, 3118−3125.

(10) Song, J. W.; Gu, W.; Futai, N.; Warner, K. A.; Nor, J. E.; Takayama, S. *Anal. Chem.* **2005**, *77*, 3993−3999.

(11) Zheng, W.; Jiang, B.; Wang, D.; Zhang, W.; Wang, Z.; Jiang, X. *Lab Chip* **2012**, *12*, 3441−3450.

(12) Unger, M. A.; Chou, H.-P.; Thorsen, T.; Scherer, A.; Quake, S. R. *Science* **2000**, *288*, 113−116.

(13) Trapnell, C.; Roberts, A.; Goff, L.; Pertea, G.; Kim, D.; Kelley, D. R.; Pimentel, H.; Salzberg, S. L.; Rinn, J. L.; Pachter, L. *Nat. Protoc.* **2012**, *7*, 562−578.

(14) Robinson, M. D.; McCarthy, D. J.; Smyth, G. K. *Bioinformatics* **2010**, *26*, 139−140.

(15) Trapnell, C.; Pachter, L.; Salzberg, S. L. *Bioinformatics* **2009**, *25*, 1105−1111.

(16) Thorsen, T.; Maerkl, S. J.; Quake, S. R. *Science* **2002**, *298*, 580−584.

(17) Gimbrone, M. A.; Topper, J. N.; Nagel, T.; Anderson, K. R.; García-Cardeña, G. *Ann. N. Y. Acad. Sci.* **2000**, *902*, 230−240.

(18) Sorescu, G. P.; Sykes, M.; Weiss, D.; Platt, M. O.; Saha, A.; Hwang, J.; Boyd, N.; Boo, Y. C.; Vega, J. D.; Taylor, W. R.; Jo, H. *J. Biol. Chem.* **2003**, *278*, 31128−31135.

(19) van der Meer, A. D.; Poot, A. A.; Feijen, J.; Vermes, I. *Biomicrofluidics* **2010**, *4*, 011103.

(20) Jo, H.; Song, H.; Mowbray, A. *Antioxid. Redox Signaling* **2006**, *8*, 1609−1619.

(21) Bongrazio, M.; Baumann, C.; Zakrzewicz, A.; Pries, A. R.; Gaehtgens, P. *Cardiovasc. Res.* **2000**, *47*, 384−393.

(22) Davis, M. E.; Cai, H.; Drummond, G. R.; Harrison, D. G. *Circ. Res.* **2001**, *89*, 1073−1080.

(23) Parmar, K. M.; Larman, H. B.; Dai, G.; Zhang, Y.; Wang, E. T.; Moorthy, S. N.; Kratz, J. R.; Lin, Z.; Jain, M. K.; Gimbrone, M. A.; García-Cardeña, G. *J. Clin. Invest.* **2006**, *116*, 49−58.

(24) SenBanerjee, S.; Lin, Z.; Atkins, G. B.; Greif, D. M.; Rao, R. M.; Kumar, A.; Feinberg, M. W.; Chen, Z.; Simon, D. I.; Luscinskas, F. W.; Michel, T. M.; Gimbrone, M. A.; García-Cardeña, G.; Jain, M. K. *J. Exp. Med.* **2004**, *199*, 1305−1315.

(25) Qiao, C.; Meng, F.; Jang, I.; Jo, H.; Chen, Y. E.; Zhang, J. *Physiol. Genomics* **2016**, *48*, 660−666.

(26) Hartmann, P.; Schober, A.; Weber, C. *Cell. Mol. Life Sci.* **2015**, *72*, 3253−3266.

(27) Brigstock, D. R. *Angiogenesis* **2002**, *5*, 153−165.

(28) Fang, Y.; Davies, P. F. *Arterioscler., Thromb., Vasc. Biol.* **2012**, *32*, 979−987.

(29) Szklarczyk, D.; Franceschini, A.; Wyder, S.; Forslund, K.; Heller, D.; Huerta-Cepas, J.; Simonovic, M.; Roth, A.; Santos, A.; Tsafou, K. P.; Kuhn, M.; Bork, P.; Jensen, L. J.; von Mering, C. *Nucleic Acids Res.* **2015**, *43*, D447−452.

(30) Wang, E. T.; Sandberg, R.; Luo, S.; Khrebtukova, I.; Zhang, L.; Mayr, C.; Kingsmore, S. F.; Schroth, G. P.; Burge, C. B. *Nature* **2008**, *456*, 470−476.

(31) Falls, D. L. *Exp. Cell Res.* **2003**, *284*, 14−30.

(32) Honda, Y.; Kondo, J.; Maeda, T.; Yoshiyama, Y.; Yamada, E.; Shimizu, Y. K.; Shikata, T.; Ono, Y. *J. Gen. Virol.* **1990**, *71*, 1999−2004.

DOI: 10.1021/acs.analchem.7b00013
Anal. Chem. 2017, 89, 3710−3715

Supporting Information

Microfluidic Device for Studying Controllable Hydrodynamic Flow Induced Cellular Responses

Chunhong Zheng[‡], Xiannian Zhang [‡], Chunmei Li, Yuhong Pang[*], and Yanyi Huang[*]

Beijing Advanced Innovation Center for Genomics (ICG), Biodynamic Optical Imaging Center (BIOPIC), School of Life Sciences, College of Engineering, and Peking-Tsinghua Center for Life Sciences, Peking University, Beijing 100871, China.

‡ These authors contributed equally (C.Z. and X.Z.).

* E-mail: pangyuhong@pku.edu.cn

* E-mail: yanyi@pku.edu.cn

This Supporting Information file includes Figures S1-S10, Tables S1-S2.

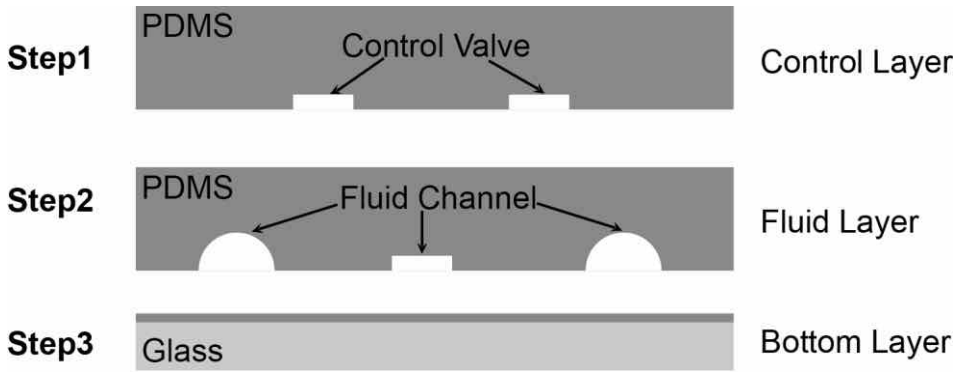

Figure S1. The schematic of chip-making procedure.

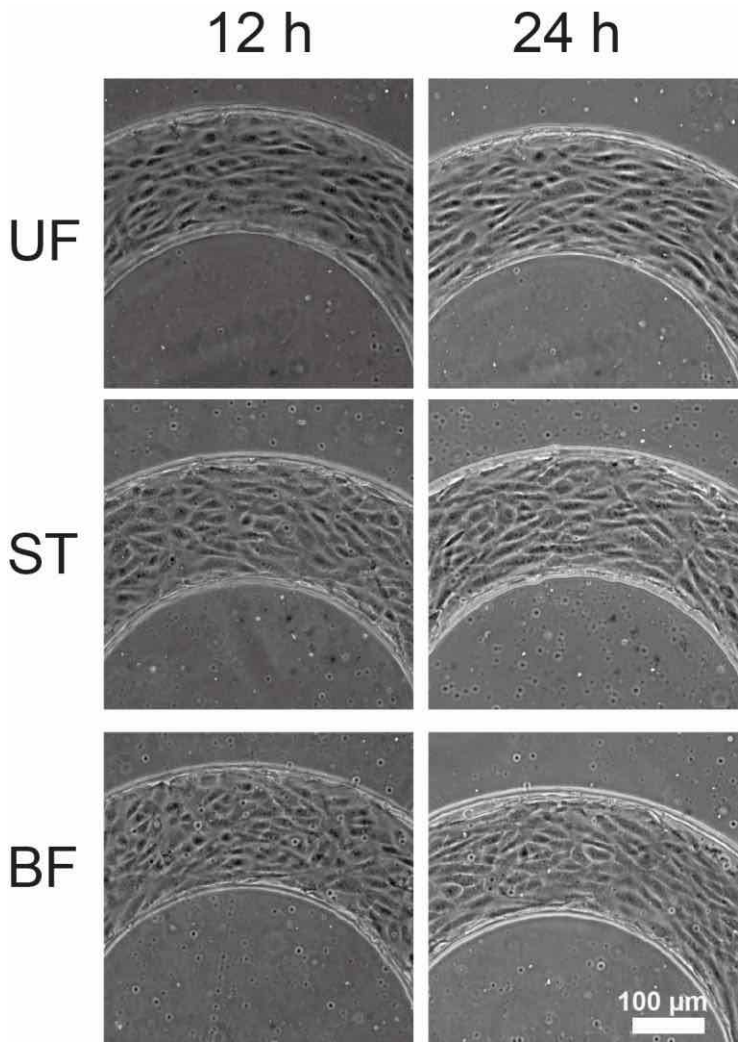

Figure S2. The morphology profile under different flow pattern. Phase contrast images show the shape of HUVECs cultured in bent channel under different flow conditions for 12 h or 24 h. UF, uni-directional flow; ST, static; BF, bi-directional flow. Scale bar, 100 μm.

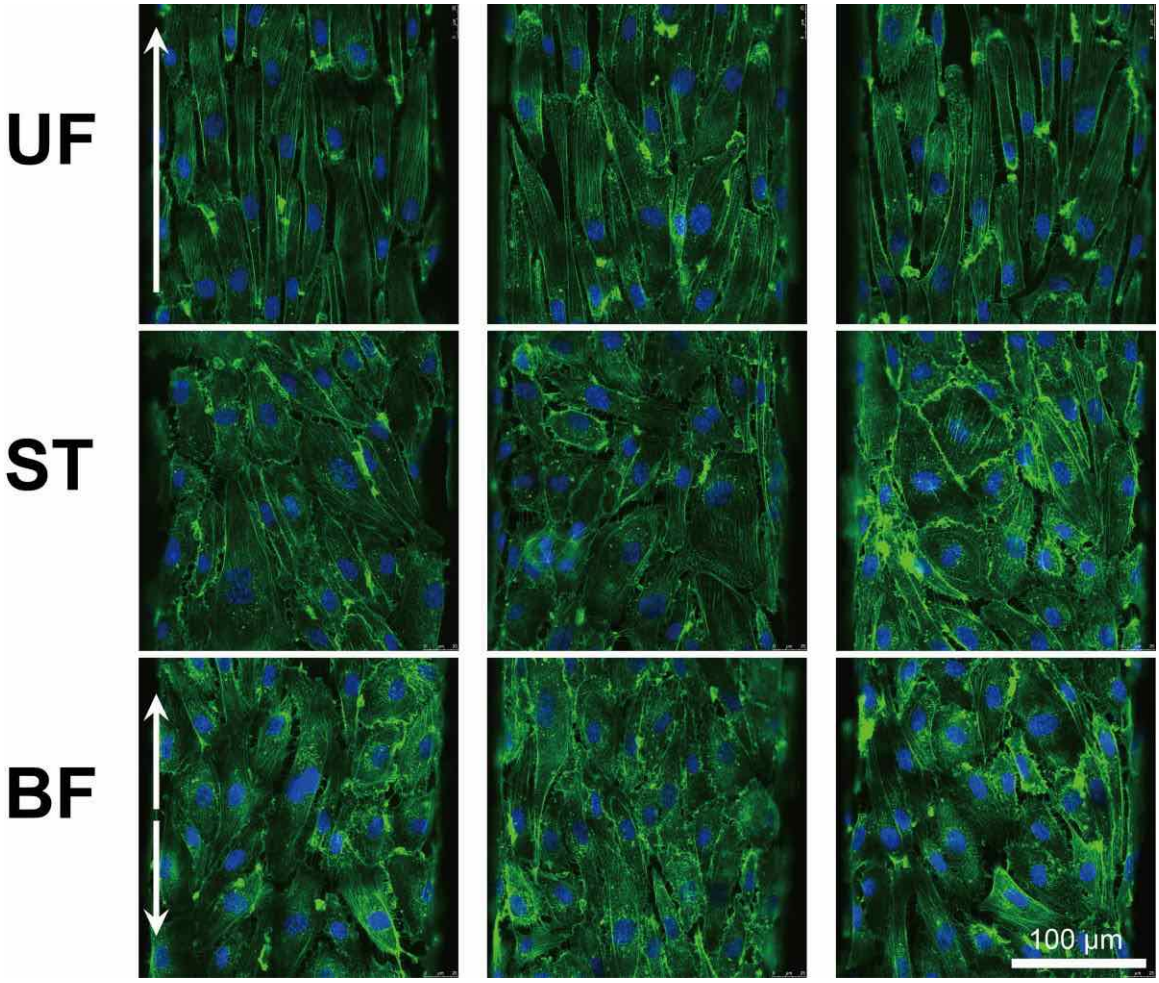

Figure S3. The confocal images of HUVECs under 24 h exposure to hydrodynamics stimulations with different flow-patterns. UF, uni-directional flow; ST, static; BF, bi-directional flow. Arrows indicate the flow directions. The nucleuses were labeled with DAPI, shown as blue; and the actins were labeled with Alexa Fluor® 555 conjugated phalloidin, shown as green.

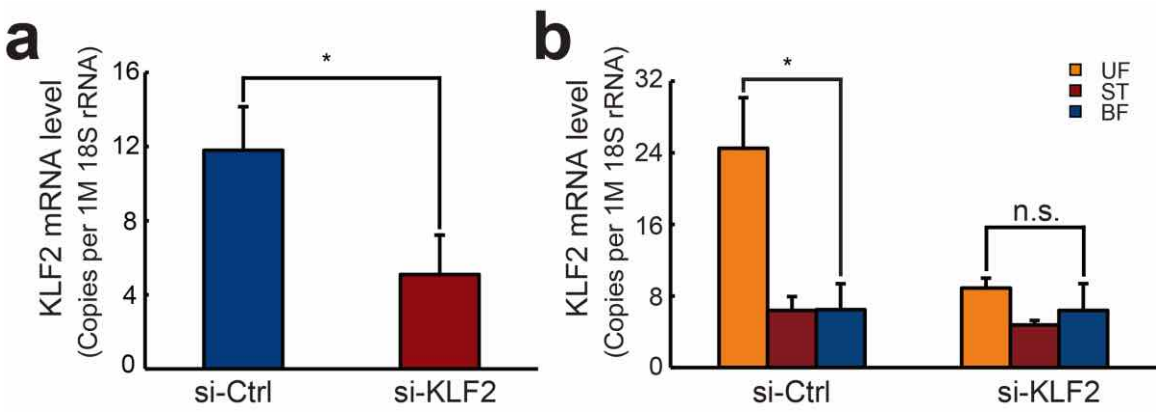

Figure S4. Expression of *KLF2* (a) before, and (b) after flow stimulations with siRNA knock-down, assessed by RT-qPCR. *, $p<0.05$; n.s., not significant.

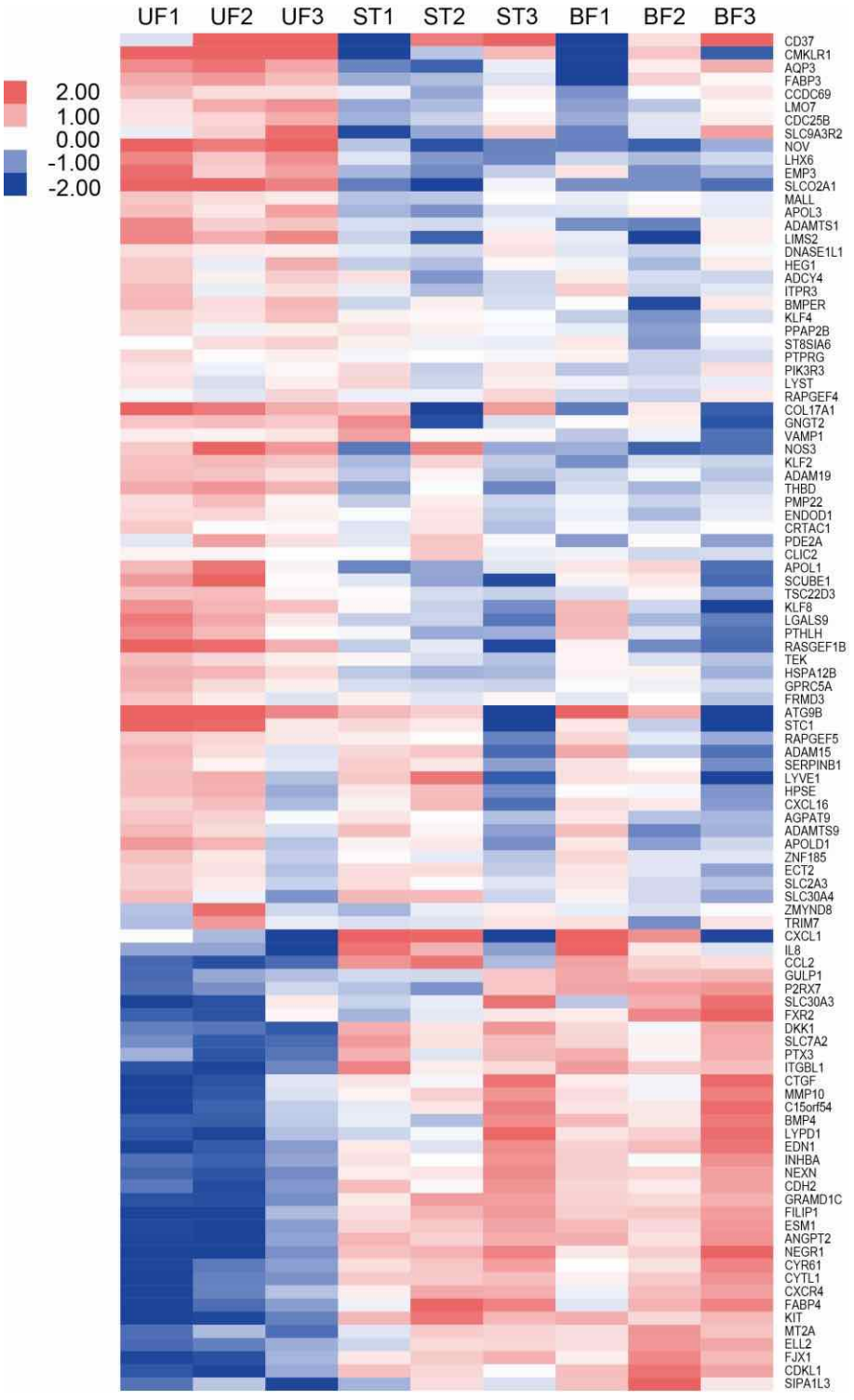

Figure S5. Heatmap showing differentially expressed mRNAs between UF- and BF-treated HUVECs.

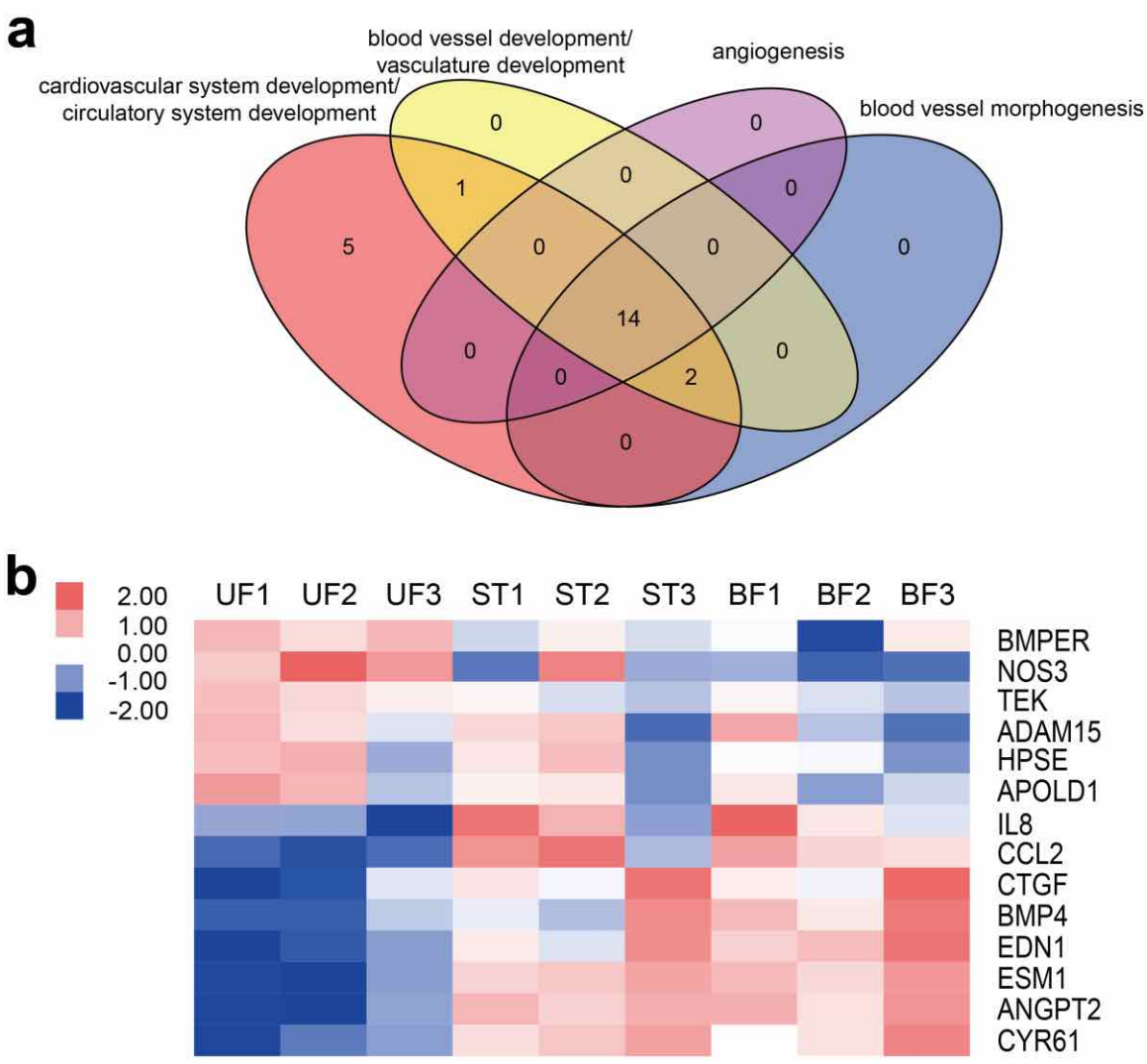

Figure S6. The overlapped genes related to blood vessel function and morphogenesis process. (a) The Venn diagram showing the overlapped genes from different biology process. (b) The heatmap showing expression of overlapped genes related to blood vessel function and morphogenesis process. UF, uni-directional flow; ST, static; BF, bi-directional flow.

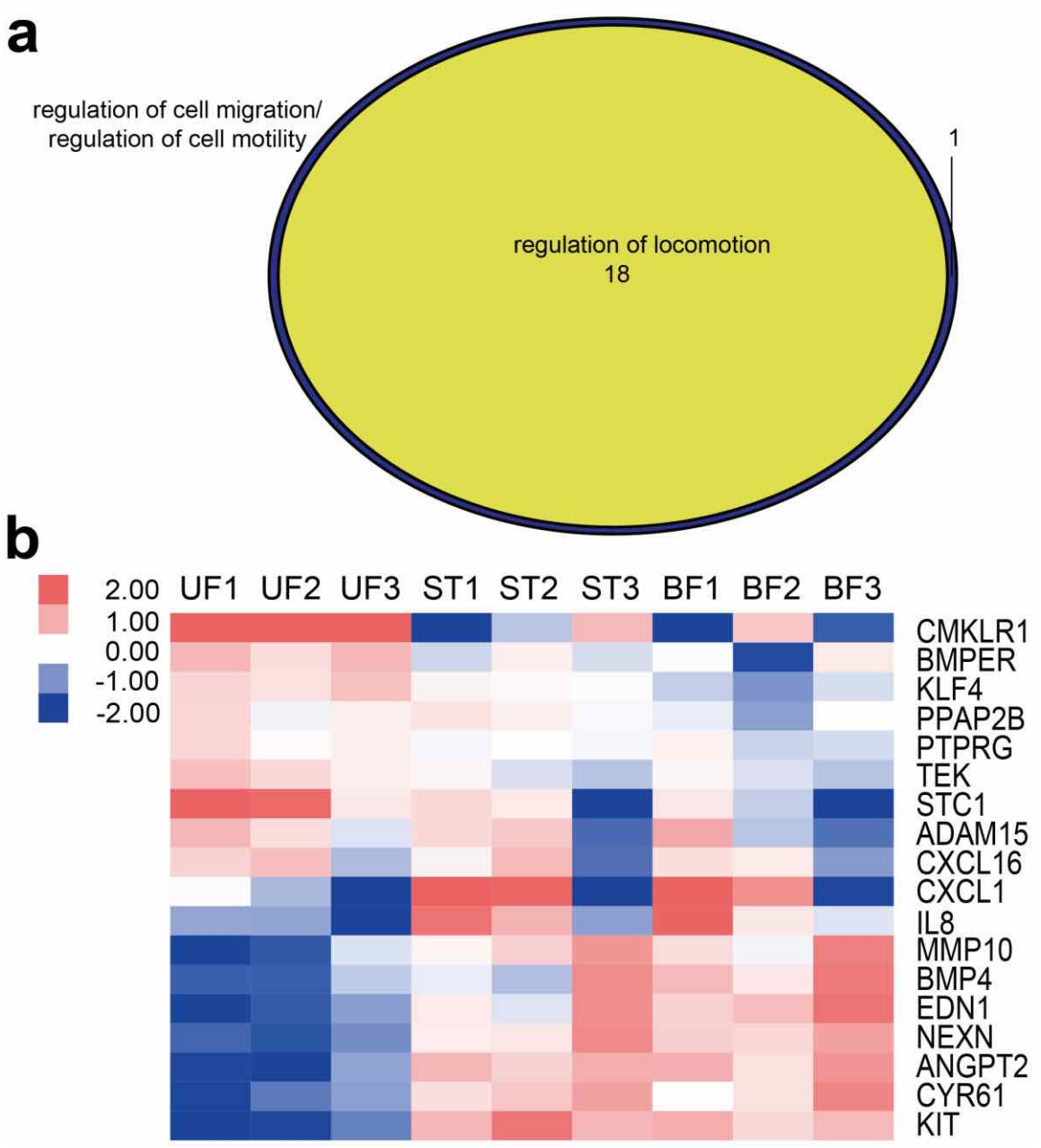

Figure S7. The overlapped genes related to cell motility. (a) The Venn diagram showing the overlapped genes from different biology process. (b) The heatmap showing expression of overlapped genes related to cell motility. UF, uni-directional flow; ST, static; BF, bi-directional flow.

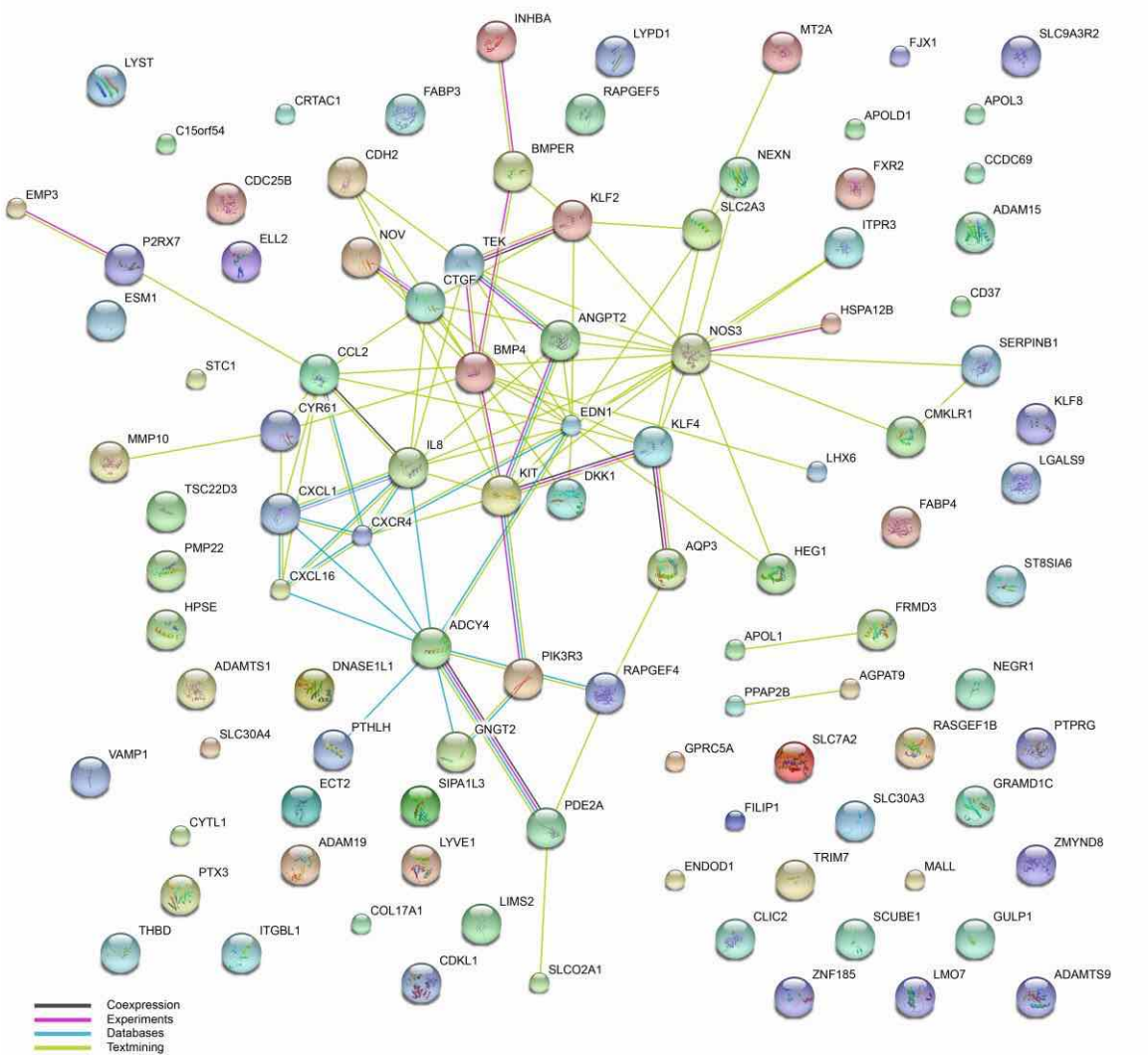

Figure S8. The closeness of relationship of 103 differentially expressed genes based on the functional roles in biological pathways, analyzed with STRING10 network diagram. The nodes indicate the individual genes and the connecting lines indicate the relationship. The shorter lines indicate closer relationship.

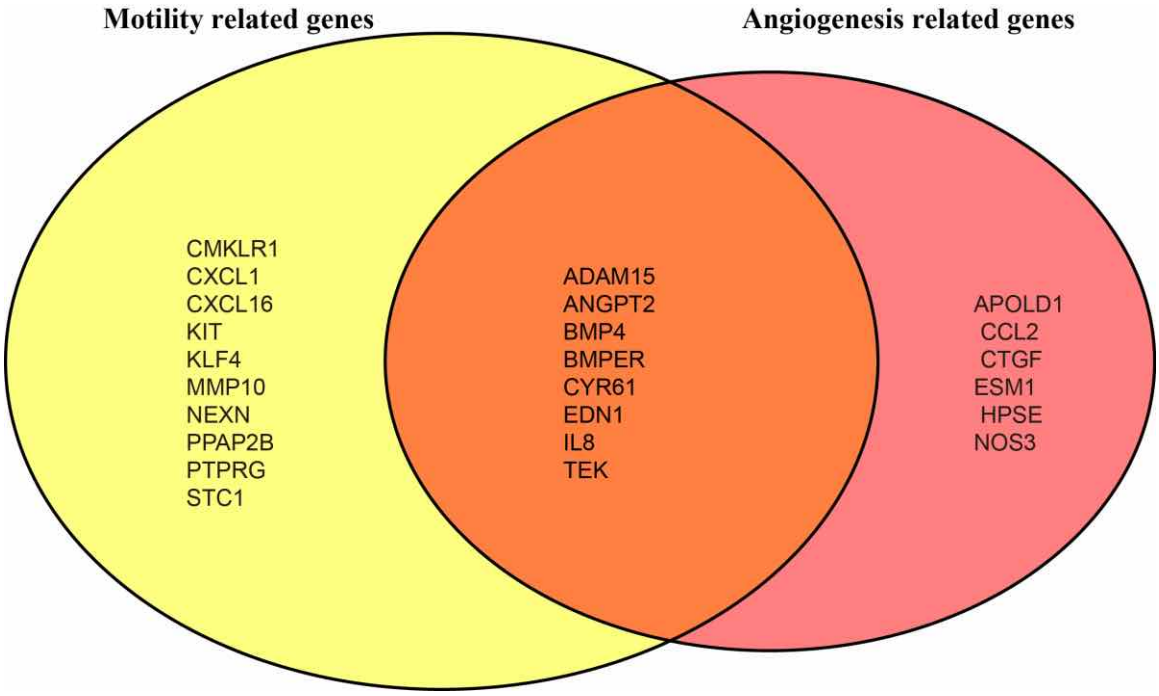

Figure S9. The Venn diagram showing the sharing genes and specific genes between motility related biology process and angiogenesis related biology process.

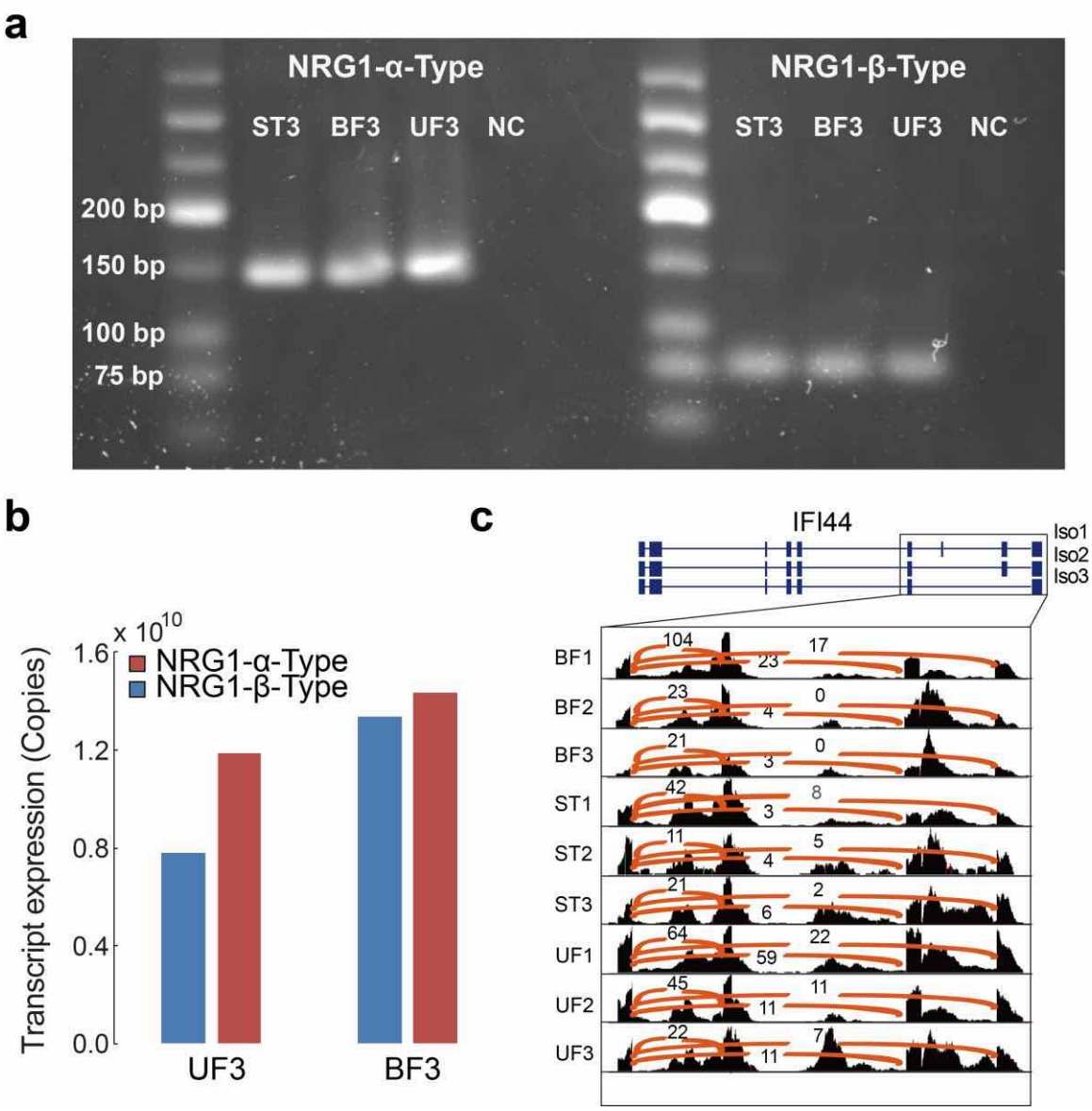

Figure S10. Flow-sensitive alternative splicing event of NRG1 and IFI44. (a) The agarose electrophoresis gel image indicating the existence of two different NRG1 transcripts. (b) The NRG1 transcripts expression after different flow pattern stimulations. UF, uni-directional flow; ST, static; BF, bi-directional flow; NC, negative control. (c) Flow-sensitive alternative splicing events in IFI44.

Table S1. Primer Sequences for RT-qPCR

Gene	Forward Primer (5' to 3')	Reverse Primer (5' to 3')
BMP4	ATGAAGCCCCCAGCAGAAGT	AGGGCTCACATCAAAAGTTTCC
NOS3	AATCCTGTATGGCTCCGAGA	GGGACACCACGTCATACTCA
ANGPT2	GAGGGACGCGCCGCTCGAAT	CCGCGTTTGCTCCGCTGTTTGG
CCL2	ACTGAAGCTCGCACTCTCGCCTCC	GCTGAGCGAGCCCTTGGGGAAT
CNN3	GGACCCAGTCGCCCAGGCAC	CGCTGGGGTCCGGGGTCTCT
MYO5A	ACCAGCAGCTCGTGCGGGTG	GGCTTCACCCCAGACACGCCC
MAP1B	TGGCATCAAGACCGGGCTGCC	TGCTTCTCAGCTGGGCTCAAGACCA
PTPRG	GCCATACTCACGCTGCAGTGCA	GACAGCAGCCAGCGTGGCCT
LYVE1	AGGCCTCCTGGCTGTCTGAGGC	GCTGAAGAAAGGGTCTGAGCTGCGG
LMO7	TGCCTGTGAGTGTGACCTCGGAGG	ACATGGCGGTTGGCCGTCCA
KLF2	AGACCTACACCAAGAGTTCGCATC	CATGTGCCGTTTCATGTGCAGC
ADAMTS1	ACACAAGGAGGATGAAACGCCGGA	ACCCCTCAGCAGCCTCCCCA
NRG1-α-type	ACATCCACCACTGGGACAAG	TCCAGTGAATCCAGGTTGGC
NRG1-β-type	GAGATACTTGTGCAAGTGCC	TGTAGAAGCTGGCCATTACGTAG

Table S2. mRNA expression (FPKM) under different flow pattern.

Gene Name	UF1	UF2	UF3	ST1	ST2	ST3	BF1	BF2	BF3
ADAM15	7.76	5.32	3.01	3.01	3.56	0.86	4.59	1.79	0.86
ADAM19	9.16	8.27	5.72	1.97	3.02	1.87	2.11	3.09	1.84
ADAMTS1	30.66	15.59	15.08	4.71	4.66	5.41	2.77	2.98	6.23
ADAMTS9	58.41	41.84	22.41	29.11	18.62	9.52	29.25	9.00	10.24
ADCY4	29.94	20.53	24.56	12.62	5.19	7.98	11.74	9.55	7.53
AGPAT9	7.21	6.19	3.67	2.88	2.39	1.61	2.81	1.86	1.44
ANGPT2	16.51	11.92	29.91	61.26	48.56	66.67	64.36	48.87	81.73
APOL1	9.36	16.44	4.67	1.23	1.57	2.38	3.25	4.42	1.03
APOL3	16.06	11.02	17.78	3.12	2.45	4.19	4.17	6.31	4.29
APOLD1	11.61	8.75	2.85	2.81	3.12	1.27	3.08	1.63	1.95
AQP3	4.74	5.57	3.08	0.41	0.33	0.84	0.14	1.22	1.74
ATG9B	4.56	4.74	2.28	0.89	0.74	0.02	2.26	1.17	0.01
BMP4	2.77	2.61	4.77	3.76	2.79	11.37	7.34	5.76	12.75
BMPER	6.52	4.51	5.43	1.45	2.09	1.54	1.81	0.59	2.12
C15orf54	0.98	1.65	3.00	2.24	3.11	7.78	3.13	3.53	9.06
CCDC69	8.30	6.19	5.35	2.35	1.49	2.88	1.26	2.94	3.07
CCL2	14.66	11.09	12.56	50.82	68.10	13.43	44.31	33.26	25.63
CD37	2.63	12.30	12.29	0.08	5.25	8.79	0.02	2.47	8.92
CDC25B	19.91	21.27	26.51	5.10	6.40	9.34	4.92	8.36	9.02
CDH2	6.11	3.81	6.28	13.27	8.00	19.46	10.63	10.32	16.29
CDKL1	3.89	2.12	6.02	10.67	8.97	6.65	10.91	25.45	13.42
CLIC2	13.49	12.71	10.49	6.47	10.34	6.02	6.08	6.01	5.13
CMKLR1	7.36	7.16	7.71	0.08	0.32	0.80	0.00	0.84	0.15
COL17A1	3.74	2.50	1.38	0.71	0.02	1.00	0.18	0.59	0.14
CRTAC1	9.36	5.68	5.25	2.67	3.92	2.13	3.02	3.20	2.99
CTGF	62.41	79.78	195.91	175.24	137.88	494.47	163.19	157.18	522.46
CXCL1	13.37	8.17	1.65	32.27	26.78	1.26	31.20	20.67	1.74
CXCL16	6.24	7.04	2.37	2.43	4.12	0.91	2.89	3.08	1.16
CXCR4	14.88	32.51	43.78	45.18	82.26	80.40	36.26	79.76	86.54
CYR61	27.60	44.46	49.59	73.48	92.31	129.86	56.38	84.18	159.32
CYTL1	1.74	2.96	2.88	5.59	5.70	6.32	3.95	6.53	9.04
DKK1	5.88	5.33	3.74	13.72	8.75	17.58	9.61	7.88	14.15
DNASE1L1	16.60	14.05	11.79	5.78	5.30	8.39	5.61	5.71	6.15
ECT2	16.80	13.97	6.53	7.75	8.06	4.45	7.37	5.95	3.23
EDN1	9.78	12.81	18.31	25.37	18.18	58.16	30.82	43.20	69.69
ELL2	13.96	15.23	18.35	14.82	25.79	26.79	24.38	54.30	39.00
EMP3	41.52	16.38	21.66	3.83	2.86	4.54	7.38	3.40	3.63
ENDOD1	4.48	4.46	3.14	1.71	2.14	1.27	1.59	1.31	1.53
ESM1	19.57	16.31	32.66	54.29	60.96	82.73	67.84	60.14	89.97
FABP3	37.57	41.31	26.65	5.76	6.38	8.21	2.22	16.08	9.55
FABP4	2.96	12.18	14.66	15.78	67.13	50.82	14.55	37.79	48.26
FILIP1	1.27	1.55	3.59	4.41	6.49	8.37	5.12	6.36	7.62
FJX1	1.23	1.40	2.58	3.05	4.03	5.01	2.83	8.37	4.48

FRMD3	6.98	4.83	3.08	2.53	1.97	2.38	1.96	2.61	1.52
FXR2	1.50	1.24	3.77	1.40	1.99	2.74	2.56	7.30	8.72
GNGT2	3.54	3.56	2.84	3.11	0.34	0.97	1.16	1.48	0.34
GPRC5A	7.14	4.95	3.59	1.64	1.60	1.55	1.95	2.16	1.53
GRAMD1C	1.98	1.82	2.67	4.01	7.84	7.85	4.87	5.33	6.40
GULP1	4.47	6.52	6.60	4.88	4.84	10.00	12.78	12.09	10.95
HEG1	25.92	14.59	27.59	6.49	5.91	9.25	8.29	6.54	9.70
HPSE	7.73	8.39	2.23	2.87	4.02	1.16	2.39	2.67	1.15
HSPA12B	10.11	9.07	5.78	1.92	1.68	1.75	2.86	3.43	1.59
IL8	5.50	5.21	1.72	17.09	9.68	2.79	19.70	7.02	4.12
INHBA	6.77	5.75	8.13	11.30	8.93	23.29	13.44	10.15	22.51
ITGBL1	1.24	0.93	1.56	6.12	2.43	2.85	4.93	3.75	3.46
ITPR3	7.45	3.70	4.58	2.02	1.46	1.78	3.30	1.96	1.88
KIT	1.86	2.97	4.39	11.33	20.76	11.45	12.33	9.74	10.70
KLF2	6.58	6.84	5.28	1.33	2.96	1.51	1.00	1.96	1.54
KLF4	15.66	13.60	15.69	6.22	6.07	5.80	4.26	3.37	4.59
KLF8	5.18	3.60	2.87	1.11	0.81	0.52	1.86	0.96	0.25
LGALS9	8.82	5.53	2.78	1.06	1.12	0.60	2.63	1.07	0.61
LHX6	3.88	2.11	3.03	0.61	0.38	0.33	0.55	0.54	0.55
LIMS2	4.51	2.99	3.69	0.63	0.30	0.98	0.74	0.18	0.92
LMO7	150.38	232.88	257.93	36.25	41.69	64.02	34.28	51.10	63.89
LYPD1	1.73	1.23	3.03	2.18	2.75	10.94	3.45	4.78	9.89
LYST	11.07	7.00	8.31	6.51	3.64	5.21	4.26	4.42	4.03
LYVE1	54.27	60.37	17.77	25.90	55.33	5.66	20.98	23.60	2.46
MALL	28.57	22.32	17.72	6.39	6.66	9.51	8.46	10.67	8.18
MMP10	19.22	25.35	57.10	46.05	62.65	107.77	55.71	46.47	124.68
MT2A	5.33	8.59	4.50	6.17	11.08	10.34	9.24	20.76	11.41
NEGR1	0.58	0.39	1.13	2.37	2.73	4.27	1.70	2.46	5.45
NEXN	1.83	1.49	1.99	3.02	3.19	7.28	3.86	4.20	5.65
NOS3	2.04	5.38	2.61	0.28	2.02	0.40	0.41	0.28	0.26
NOV	49.62	22.21	31.60	2.69	1.17	1.77	1.70	1.58	2.23
P2RX7	1.32	1.57	2.20	1.20	0.88	2.79	3.77	4.59	4.21
PDE2A	4.98	12.16	6.19	2.62	4.84	2.96	1.57	3.51	1.60
PIK3R3	22.77	16.41	16.40	13.24	7.36	12.03	6.72	8.52	12.15
PMP22	200.35	256.79	140.26	59.27	90.50	63.06	76.15	71.43	68.62
PPAP2B	11.77	7.69	8.14	5.66	4.99	4.38	3.99	2.80	4.34
PTHLH	6.25	3.89	1.98	1.16	0.71	0.74	2.05	1.19	0.46
PTPRG	16.50	11.67	11.06	5.93	6.29	6.06	6.74	5.46	4.82
PTX3	128.48	64.05	72.06	210.67	94.45	194.45	215.83	136.48	207.07
RAPGEF4	6.37	5.56	7.84	3.20	3.25	4.92	2.72	3.02	4.01
RAPGEF5	62.34	51.66	39.61	22.98	20.77	9.28	27.70	20.84	11.73
RASGEF1B	7.49	6.47	3.00	0.71	0.86	0.26	1.05	0.53	0.36
SCUBE1	3.49	8.70	1.27	0.67	0.44	0.22	0.82	1.07	0.28
SERPINB1	18.20	11.22	8.02	8.41	6.93	3.15	7.08	6.77	2.63
SIPA1L3	1.39	2.34	0.73	1.13	2.36	1.52	3.01	21.02	2.14
SLC2A3	64.45	50.01	27.75	29.68	23.38	19.87	27.18	21.20	15.36
SLC30A3	1.45	1.74	5.85	2.36	2.86	10.75	2.19	7.18	10.43

SLC30A4	9.50	4.91	2.34	5.26	5.15	2.27	3.15	2.68	1.59
SLC7A2	5.54	3.76	3.73	13.90	7.71	10.57	8.42	7.73	11.76
SLC9A3R2	9.79	15.11	32.61	1.52	3.26	8.51	2.50	5.56	12.12
SLCO2A1	4.00	2.57	1.25	0.11	0.05	0.25	0.13	0.15	0.10
ST8SIA6	4.30	5.42	5.21	2.50	2.10	2.05	2.63	1.35	1.94
STC1	103.07	82.87	23.27	16.62	14.41	1.91	14.43	10.36	2.55
TEK	57.95	44.18	32.24	18.74	14.75	12.40	18.74	17.04	11.86
THBD	23.16	26.78	17.68	3.31	5.88	2.73	4.76	4.34	4.46
TRIM7	3.37	11.52	3.87	2.22	2.26	3.30	3.33	1.49	3.15
TSC22D3	41.75	41.47	21.89	13.18	10.69	9.83	10.77	15.83	7.39
VAMP1	3.45	3.16	3.11	3.52	1.63	1.70	1.11	1.71	0.61
ZMYND8	15.19	79.20	14.76	7.33	10.59	13.39	10.40	11.34	11.50
ZNF185	11.40	7.86	4.24	3.63	3.21	2.51	4.88	3.57	2.95